GNN-RAP: Joint Uplink-Scene Fusion for Cross-Frequency mmWave and THz Channel Path Prediction in FDD networks

Jui Mhatre, Ahyoung Lee*
Department of Computer Science, Kennesaw State University, Marietta, GA 30060, USA.
Email: jmhatre1@students.kennesaw.edu, *ahyoung.lee@kennesaw.edu. (*Corresponding Author)

***Abstract*—Ray tracing simulations are widely regarded as a benchmark approach for high-fidelity propagation modeling, enabling accurate design and validation of 5G and beyond-6G networks, yet remain computationally prohibitive for real-time applications. Sionna RT and similar tools require milliseconds per link, scaling poorly for large-scale simulations and online channel state prediction. Neural surrogates have emerged to accelerate ray tracing by orders of magnitude. Existing approaches assume high uplink-downlink (UL-DL) path congruence and require full 3D scene geometry, which is unrealistic for frequency division duplex (FDD) systems spanning sub-6 GHz uplink to mmWave/sub-THz DL. This makes predicting DL paths using UL paths less complex. But the complexity increases when path congruence degrades in cross bands UL-DL communication. Using Sionna ray tracing in Munich's urban environment, with low path congruence and limited scene geometry, we propose the AI-based ray tracing surrogate for non-reciprocal FDD. In our FDD system, we consider large frequency gaps between UL (3.5 GHz) and DL (300 GHz) that generate only 40% of overlapping paths. Our proposed approach, graph neural network for radio access path prediction (GNN-RAP) that encodes sub-6 GHz UL paths and coarse environmental geometry knowledge to predict mmWave/sub-THz DL multipath components. We compare the predicted paths with the state-of-the-art OptML [1] model as well as with true DL paths. GNN-RAP reduces prediction error by 3-4× versus OptML while scaling in dense urban scenes. By exploiting environmental structure, it overcomes UL-DL duality limits, enabling real-time beam management for frequency-agnostic 5G/6G systems without dense DL pilots.**

***Index Terms*—Path prediction, Graph neural network, Phase, Large frequency gap, Delay, Jaccard index, Frequency division duplex.**

I. Introduction

Ray tracing is a site-specific channel modeling framework in 5G and emerging 6G system design [2]. Tools such as NYURay and Sionna RT load three-dimensional geographic information system (GIS) data (e.g., OpenStreetMap building footprints, heights, and materials); launch rays from transmitters; trace reflections, diffractions, and transmissions through the environment; and reconstruct multipath channel coefficients at arbitrary carrier frequencies using electromagnetic propagation models [2]–[4]. This level of fidelity enables high-confidence validation of beamforming and link adaptation schemes, the construction of realistic digital-twin networks (DTNs) [5].

ISBN 978-3-903176-82-9 ©2026 IFIP

However, ray tracing's accuracy comes at a computational cost. A typical Sionna RT simulation can take from several milliseconds to seconds per link on a GPU, depending on scene complexity, requested number of paths, and frequency bands [2]. Additionally, these methods depend in channel state information reference signals (CSI-RS) for channel estimation and path extraction, which is energy intensive. As 6G research pushes toward intelligent reflecting surfaces, highly directional mmWave/sub-THz links, and ultra-dense deployments, there is a clear need for faster yet still physically grounded, AI-based propagation models that capture path-level structure [6], [7].

Neural ray tracing represents an emerging paradigm to address the computational bottleneck of traditional ray tracers by training deep networks to approximate their input-output mapping. WiNeRT [8], is among the earliest works, predicts multipath parameters (angles of arrival/departure, delays, and gains) from 3D scene representations and transmitter/receiver positions. A more recent neural ray tracing approach trains multi-layer perceptrons on datasets generated by Sionna RT to predict path gains, time of flight, and angles in the Munich urban scenario [9]. KANNA-NeRF [10] advances this line by combining Kolmogorov-Arnold networks (KANs) with neural radiance field (NeRF) techniques for volumetric propagation modeling, achieving near-perfect overlap between uplink (UL) and downlink (DL) channel frequency responses in controlled indoor WiGig scenarios (60 GHz).

Physics-informed neural networks (PINNs) and surrogate modeling techniques offer additional perspectives on propagation prediction. PINNs for channel estimation combine model-based priors (e.g., sparsity, low-rank structure) with deep learning in pilot-limited scenarios. GeNeRT [11] incorporates physics constraints into neural ray tracing for improved indoor generalization. While these approaches improve sample efficiency and generalization, they remain largely single-band or moderate-diversity, assuming frequency-invariant geometry or shared propagation paths across bands. They do not address the explicit path divergence that occurs in large-gap FDD.

A complementary line of research targets cross-band CSI prediction specifically for Frequency Division Duplexing (FDD) systems, aiming to leverage UL CSI at one frequency to inform DL beam selection, channel estimation, or precoding at another frequency. The seminal R2-F2 [12] system employs convolutional neural networks (CNN) to map sub-

6 GHz beam indices to mmWave beams. OptML [1] takes a gradient-descent approach, optimizing DL channel estimates within UL-derived subspaces , typically in moderate frequency gaps ($\leq$30 MHz). More recently, HORCRUX [13] introduces frequency-aware CNN fusion for measured sub-6 28/39 GHz channel pairs. However, they operate primarily in the CFR or beam domain, regressing entire channel matrices. Moreover, they provide little insight into performance degradation as UL-DL frequency separation increases or as path overlap diminishes, leaving users without guidance on when UL-based prediction is physically viable.

The literature reveals three critical gaps:

- *Large-frequency-gap path divergence:* No prior neural ray tracing or cross-band CSI work systematically evaluates path prediction across large frequency gaps, where NLOS congruence collapses, exposing fundamental physical limits on UL-based prediction.
- *Pilot signal dependence:* DL paths estimation from channel is done using energy-consuming CSI-RS pilot signals.
- *Practical deployment constraints:* Neural-RT methods require full 3D scene meshes that are unavailable in real-time FDD CSI acquisition; cross-band predictors assume high UL-DL overlap without path-level decomposition or practical input proxies.
- *Independent-path regimes:* Existing models do not handle "independent-solve" scenarios (separate UL/DL ray traces reflecting FDD reality) or quantify the relationship between measured path overlap and prediction fidelity for adaptive system design.

This paper fills these gaps with a graph neural network for radio access path prediction (GNN-RAP), the first AI-based ray tracing surrogate for non-reciprocal FDD. The novelty of this paper lies in DL pathfinding in a large UL-DL frequency gap network with cross-band communication without any pilot signals. This paper makes the following main contributions to the emerging area of AI-based ray tracing:

- *Quantitative Congruence Benchmark for Large-Gap FDD ($\approx$295 GHz):* We systematically measure and characterize UL to DL path overlap using Sionna RT in the Munich urban scenario across multiple DL bands. We report cluster Jaccard indices, angular power spectrum (APS) correlations, and DL power fractions near UL-dominant directions, providing the quantitative evidence of path divergence in large-gap FDD.
- *AI-Based Ray Tracing Surrogate Architecture for Non-Reciprocal FDD:* We propose GNN-RAP, a geometry-aware neural model that encodes observed UL paths and coarse environment geometry features to generate DL multipath components. We evaluate frequency-sensitive path parameters such as phase, delay, and power.
- *Computational Speedup with Practical Deployability:* Unlike neural ray tracing methods that require full 3D scene meshes, our approach uses only UL path observations (extractable from standard channel sounders) and basic geometric features (pre-deployed as OpenStreetMap), enabling deployment in live FDD systems without GIS mesh dependencies, achieving effective speedup while maintaining physics-ceiling awareness.
- *Path-Space Decomposition and Attribution:* Unlike prior cross-band CSI works that treat DL holistically, we explicitly decompose DL paths and power into UL-related and UL-independent components, enabling clear attribution of which DL energy can be explained by UL and which must be inferred from geometry alone, providing physical insight into the limits of reciprocity-based prediction at large frequency gaps.

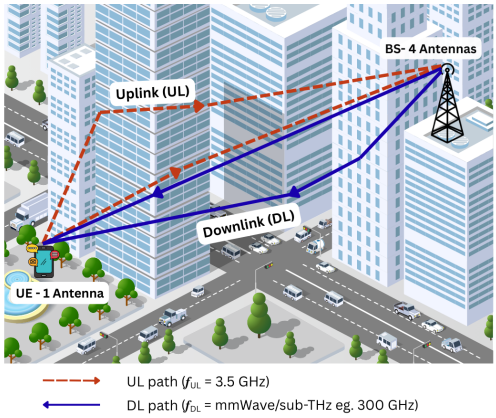

Fig. 1: Frequency division duplex network with a large frequency gap causing different UL and DL paths.

The rest of this paper is organized as follows. Section II details the system model, ray tracing setup, path extraction pipeline, and geometry feature construction. Section III presents the UL-DL path congruence analysis and discusses its implications. Section IV describes the GNN-RAP architecture and training objectives. Section V describes dataset generation and performance metrics followed by path-level evaluation resultss, and Section VI concludes the paper with future work.

II. System Model

Consider a FDD wireless system with separate UL and DL frequency bands. This allows simultaneous UL and DL transmission on different carriers, enabling symmetric or asymmetric traffic patterns. The key challenge in cross band FDD is the lack of instantaneous reciprocity as shown in Fig. 1: the UL channel at frequency f_{UL} does not directly mirror the DL channel at frequency f_{DL} due to frequency-dependent propagation phenomena. In this work, we focus on cross band large frequency gap FDD, where the UL operates at sub-6 GHz (specifically 3.5 GHz, typical for the cellular n78 band) and the DL operates at mmWave or sub-THz frequencies (28, 40,... 300 GHz). Such large frequency gaps between UL and DL induce severe non-reciprocity of paths because material properties, diffraction efficiency, and scattering mechanisms vary dramatically across this range.

The wideband channel between BS and UE can be modeled as a sum of multipath propagation components k. At the UL

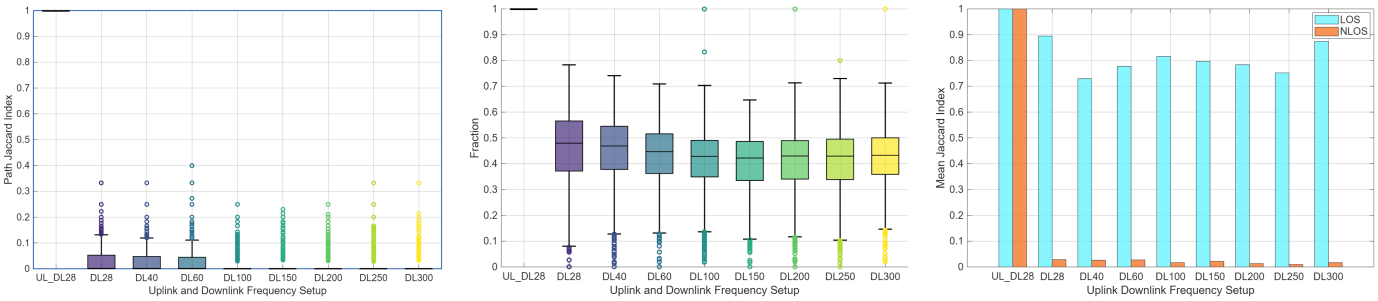

(a) Path Cluster Jaccard Index (b) Fraction of DL with UL Neighbors (c) LoS vs. NLoS

Fig. 2: Path Congruence comparison for uplink and downlink paths at various frequencies. UL_DL 28 denote both UL and DL operate at same frequency of 28 GHz, all others, DL_X, denote UL at 3.5 GHz and DL at X GHz.

frequency f_{UL}, the received signal [14] is,

$$y_{UL}(t) = \sum_{k=1}^{P_{UL}} \alpha_k^{UL} s(t - \tau_k^{UL}) e^{j2\pi f_{UL} \phi_k^{UL}} + w(t), \quad (1)$$

where α_k^{UL} the complex path gain, τ_k^{UL} is the propagation delay, ϕ_k^{UL} is the phase shift, $s(t)$ is the transmitted waveform, and $w(t)$ the additive noise. Similarly, at the DL frequency f_{DL},

$$y_{\mathrm{DL}}(t) = \sum_{k=1}^{P_{\mathrm{DL}}} \alpha_k^{\mathrm{DL}} s_k(t - \tau_k^{\mathrm{DL}}) e^{j2\pi f_{DL} \phi_k^{DL}} + w(t). \quad (2)$$

The UL and DL signals are characterized by the angle of arrival at the receiver $(\varphi_{r,k}, \theta_{r,k})$ in azimuth and elevation and the angle of departure (AoD) at the transmitter: $(\varphi_{t,k}, \theta_{t,k})$ in azimuth and elevation. The frequency-domain channel [15] can be expressed using angular-delay representation,

$$H(f) = \sum_{k=1}^{P} \alpha_k(f)\, \mathbf{a}_{\mathrm{R}}(\varphi_{r,k}, \theta_{r,k})\, \mathbf{a}_{\mathrm{T}}^{\mathrm{H}}(\varphi_{t,k}, \theta_{t,k})\, e^{-j2\pi f \tau_k}, \quad (3)$$

where $\mathbf{a}_{\mathrm{R}}(\cdot)$ and $\mathbf{a}_{\mathrm{T}}(\cdot)$ are receive and transmit array response vectors, and the complex path gain $\alpha_k(f)$ are frequency dependent due to material absorption, diffraction attenuation, and penetration losses [6], [16]. Path-dependent parameters, τ_k normalized delay, and ϕ_k is phase shift vary when UL and DL paths are different. Thus, in our scenario for cross band, the UL and DL frequencies are very far apart, and both frequency and path-dependent parameters are different. The larger the gap, the more is the variation. Due to frequency-dependent material responses, penetration depths, and scattering cross-sections, the set of dominant propagation paths at f_{UL} differs significantly from those at f_{DL} when $f_{\mathrm{DL}} \gg f_{\mathrm{UL}}$ [17].

III. Problem Statement

In this paper, we address the problem of predicting DL path structure purely from UL observations and coarse environment geometry, without any pilot signals for DL CSI feedback, in a large frequency gap cross band FDD system. Research [12] show that the DL channel can be predicted from UL counterparts, thereby reducing costly DL pilots and feedback. Our analysis in Fig. 2, however, shows that this assumption fails in FDD systems with large frequency gaps, over 28 GHz. At large frequency gaps such as in cross band communication, the UL-DL covariance is very high, thus prediction DL from UL becomes very complex. We measured path overlap as a measure of cluster Jaccard index in joint delay angle space in Fig. 2(a). In the first measurement, both UL and DL frequencies are 28 GHz; then we clipped UL to 3.5 GHz and changed DL from 28 GHz to 300 GHz. We observe that when UL and DL operate in the same frequency, the Jaccard index (JI) is near to 1.0, indicating high path congruence, but it collapses sharply once UL and DL frequencies diverge, and JI reaches close to zero. This was exact matching of angles and delays. We further relaxed the matching such as to allow angular separation of $\pm 10^{\circ}$ in Fig. 2(b). The results indicate, matching is 1.0 for same band communication, but dropping below 45% when frequencies diverge. Further, we investigated paths that change path direction in Fig. 2(c). It shows that, for the same frequency, both LoS and NLoS path directions are the same, but as the frequency gap widens, the majority of the DL NLoS structure is effectively independent of the UL. Consequently, any method that attempts to reconstruct the full DL channel directly from UL, it can at best recover the small fraction of DL power that is UL-related, while the bulk of DL energy arises from frequency-specific NLoS paths that cannot be inferred deterministically from UL alone.

IV. Proposed Solution

Our proposed solution, graph neural network for radio access path (GNN-RAP) for DL path prediction as a conditional generative problem in which a neural network learns to synthesize a set of dominant DL multipath components from observed UL paths and coarse scene information as shown in Fig. 3, without requiring any DL pilots or full 3D meshes. Since Ray tracing frameworks use the predicted paths for channel estimation, we predict path parameters rather than entire paths: phase, path power, and delays [18], [19].

For each link we collect the top-K UL paths p_k^{UL} as a matrix, $\mathbf{X}^{UL} \in \mathbb{R}^{K \times 5}$, where $p_k^{UL} = \{\varphi_{r,k}, \theta_{r,k}, \tau_k, \alpha_k, \phi_k\}$, and a scene graph descriptor is $\mathbf{G}$ built from the transmitter, receiver, and scatterer objects encoded as node features and

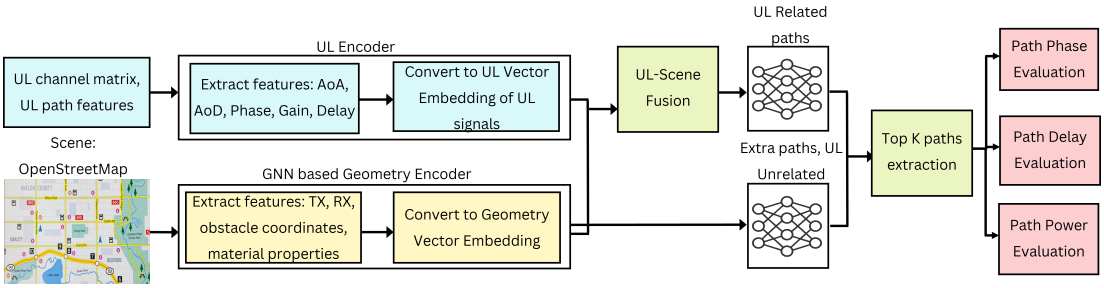

Fig. 3: Graph neural network for radio access path prediction (GNN-RAP): uplink and geometry encoded, downlink decoder.

edges. We implement a dual head model to predict DL paths. In the first part, we predict paths related to UL using f_θ,

$$f_\theta = (\mathbf{X}^{UL}, \mathbf{G}, z) \mapsto \hat{Y}^{DL} \in \mathbb{R}^{K \times d_{path}}, \tag{4}$$

where $z \sim \mathcal{N}(0, I)$ is a low-dimensional noise vector and each row of $\hat{Y}^{\mathrm{DL}}$ is a predicted DL path $\hat{p}_k^{\mathrm{DL}} = (\hat{\varphi}_{r,k}, \hat{\theta}_{r,k}, \hat{\tau}_k, \hat{\rho}_k, \hat{\phi}_k)$, comprising azimuth, elevation, normalized delay, log power fraction ($\hat{\rho}_k = |\hat{\alpha}_k|$), and phase, thus $d_{path} = 5$. The second part predicts paths not related to UL signals. The architecture consists of three main components: a UL path encoder, a scene graph encoder, and a shared decoder to finally predict DL paths with two heads explained above.

The UL path encoder applies a small multilayer perceptron (MLP) with shared weights across paths, then pools over the K paths to obtain a fixed-length embedding

$$\mathbb{E}^{\mathrm{UL}} = \mathrm{Pool}\big(\sigma\big(W_2\,\sigma\big(W_1 X^{\mathrm{UL}} + b_1\big) + b_2\big)\big) \in \mathbb{R}^{d_{\mathrm{UL}}}, \tag{5}$$

where $\sigma(\cdot)$ is a nonlinearity (e.g., GELU/ReLU), W_1, W_2 and b_1, b_2 are trainable weights, and $\mathrm{Pool}(\cdot)$ is a permutation-invariant operation such as mean or max over the paths.

In parallel, the scene graph encoder using graph neural network (GNN) learns how the receiver's position relative to TX and scatterers influences the DL paths, enabling context-aware path predictions. It represents the environment as node features $V \in \mathbb{R}^{N \times d_{geom}}$ (TX, RX, and obstacles) and an edge index $E \subset \{1, \ldots, N\}^2$, where $d_{geom} = 9$ is geometric dimensions, and performs graph message passing to obtain edges given by,

$$\mathbb{E}_i^{(l+1)} = \sigma\left(W^{(l)}\mathbb{E}_i^{(l)} + \sum_{j:(j,i)\in E} \Phi^{(l)}\left(\mathbb{E}_j^{(l)}, \mathbb{E}_i^{(l)}\right)\right), \tag{6}$$

starting from $\mathbb{E}_i^{(0)} = V_i$ and stacking several layers $l = 0, \ldots, L-1$. A global pooling over nodes then yields a geometry embedding

$$\mathbb{E}_{\mathrm{geom}} = \mathrm{Pool}_i\left(\mathbb{E}_i^{(L)}\right) \in \mathbb{R}^{d_{\mathrm{geom}}}. \tag{7}$$

The joint latent representation is obtained by concatenating the UL, geometry, and noise vectors,

$$\mathbb{E} = \left[\mathbb{E}^{\mathrm{UL}} \,\|\, \mathbb{E}_{\mathrm{geom}} \,\|\, z\right] \in \mathbb{R}^{d_{\mathbb{E}}}, \tag{8}$$

and expanding it through a shared decoder trunk to produce K path embeddings

$$\mathbb{E}_{\mathrm{path}} = \mathrm{ResMLP}(h) \in \mathbb{R}^{K \times d_{\mathrm{path}}}, \tag{9}$$

where ResMLP denotes a stack of fully connected layers with residual connections, reshaping $\mathbb{R}^{d_{\mathbb{E}}}$ into $\mathbb{R}^{K \times d_{\mathrm{path}}}$. A final linear layer maps each path embedding $\mathbb{E}_k^{\mathrm{path}}$ to raw outputs of DL paths represented as,

$$\tilde{y}_k = W_{\mathrm{out}}\mathbb{E}_k^{\mathrm{path}} + b_{\mathrm{out}} \in \mathbb{R}^5, \tag{10}$$

which are interpreted as unconstrained azimuth, elevation, delay log-coordinate, power logits, and phase. To enforce geometric validity and power conservation, these raw outputs are passed through deterministic bounding transforms before being used as paths. The azimuth and elevation are via, $\hat{\varphi}_{r,k} = \tanh(\tilde{y}_{k,1}), \hat{\theta}_{r,k} = \tanh(\tilde{y}_{k,2})$, ensuring they lie in the normalized range $[-1, 1]$ that maps back to $[-\pi, \pi]$ and $[-\pi/2, \pi/2]$, respectively. The normalized delay coordinate is similarly constrained to $[0, 1]$ by clipping the values accordingly as,

$$\hat{d}_k = \mathrm{clip}(\tilde{y}_{k,3}, 0, 1), \tag{11}$$

and later denormalized per sample using stored delay minima and ranges to recover absolute delays through a log-scale inverse mapping. Power is parameterized via a log-softmax over the K paths,

$$\hat{\ell}_k = \log \frac{\exp(\tilde{y}_{k,4})}{\sum_{j=1}^{K} \exp(\tilde{y}_{j,4})}, \tag{12}$$

so that $\exp(\hat{\ell}_k)$ are power fractions that sum to one across k and can be scaled by the total DL power to obtain per-path powers in linear or logarithmic domain. Finally, the phase output is treated as an angle on the complex unit circle, $\hat{\phi}_k = \angle(\exp(j\tilde{y}_{k,5}))$, which wraps the unconstrained real value back into $[-\pi, \pi]$. Overall, the network implements the mapping,

$$(X^{\mathrm{UL}}, G, z) \mapsto \left\{(\hat{\varphi}_{r,k}, \hat{\theta}_{r,k}, \hat{d}_k, \hat{\ell}_k, \hat{\phi}_k)\right\}_{k=1}^{K}, \tag{13}$$

where the UL encoder learns which UL angles and powers are predictive of DL structure, the graph encoder captures how BS-UE distance and scatterer layout constrain feasible propagation paths, and the decoder fuses these embeddings with noise into a valid set of DL paths whose geometry, delay, power allocation, and phase can be used to synthesize DL.

TABLE I: Simulation parameters

Parameter	Value
Scene / environment	Sionna-RT Munich 3D urban
BS antennas	1×4 planar array (TR 38.901 pattern)
UE antennas	1
UL carrier frequency f_{UL}	3.5 GHz
DL carrier frequency f_{DL}	28, 40, 60, 100, 150, 200, 250, 300 GHz
FFT size / subcarriers	128
Subcarrier spacing	30 kHz
OFDM symbols per slot	12
Number of UE positions	1000
Maximum dominant paths	8

The training objective incorporates a carefully designed loss function that balances multiple complementary aspects of path parameter prediction. The total loss is computed as a weighted sum of distinct loss components, each targeting a specific aspect of the multipath prediction problem. The reconstruction loss measures the Kullback-Leibler divergence between the predicted power fractions and the ground truth power distributions. The geometric loss computes the mean squared error between predicted and true angles as well as the normalized delay parameters. A novel component introduced in this work is the PHI-specific loss, which targets the azimuth angle prediction accuracy. The phase loss measures the circular phase error between predicted and true phase values. The Hungarian matching loss addresses the combinatorial challenge of establishing correspondence between predicted and true paths and evaluating the parameters.

V. Results and Discussion

We implement an intelligent model for DL path prediction based on UL paths and environment geometry. The dataset is generated using Sionna ray tracing in the Munich scenario with 1000 independent BS-UE links, where UL and DL is at different frequencies using frequency-dependent material properties (brick, concrete, glass) with ray tracing parameters. OpenStreetMap data are used to generate the environment geometry consisting of various obstacles, TX/RX coordinates, material, material characteristics, etc. Simulation parameters used in our scene are summarized in Table I. To assess the prediction quality, multiple metrics were computed comparing the model predictions against ground truth values and the existing state-of-the-art solution, OptML [1].

We evaluate our proposed GNN-RAP model on the validation set for the extreme cases of 3.5 to 28 GHz (moderate gap) and 3.5 to 300 GHz (large gap). Our results show estimates of the predicted delay, phase, and power distributions versus Sionna RT ground truth and OptML, demonstrating that GNN-RAP consistently achieves tighter alignment with ground truth across both frequency gaps. These visualizations reveal the models' ability to capture the marginal statistical structure of ray-traced DL paths despite operating in a low-congruence regime where NLOS path overlap is near zero. Power distributions in Fig. 4 capture the 40 to 60 dB dynamic range of ray-traced paths. True DL power distribution shows mean of -103.96 dB for UL-DL frequency gap of 25 GHz and

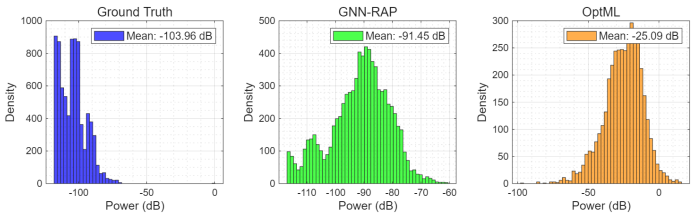

(a) Uplink: 3.5 GHz, Downlink: 28 GHz

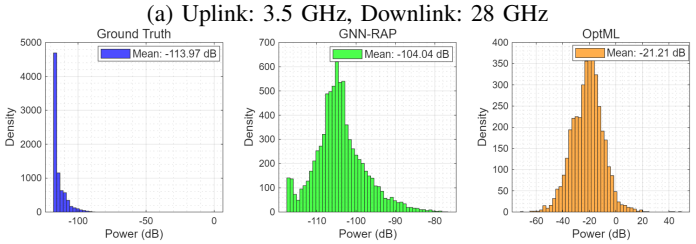

(b) Uplink: 3.5 GHz, Downlink: 300 GHz

Fig. 4: Path power prediction distribution.

-113.96 dB for 295 GHz. GNN-RAP predicted DL paths with MAE of 12.5 dB and 9.9 dB for frequency gap of 25 GHz and 295 GHz respectively. OptML produces MAE of 78.9 dB for DL paths at 28 GHz and 92.8 dB at 300 GHz reflecting its UL-only design's complete failure to learn frequency-dependent path loss scaling trained on moderate gaps.

Phase distributions in Fig. 5 shows uniform ground-truth spreads on $[-\pi, \pi]$ due to random scatterer phases and propagation geometry. GNN-RAP achieves the closest match, with MAE of 0.13 rad and 1.36 rad for DL paths at 28 GHz and 300 GHz respectively, and minimal bias, preserving the uniform spread essential for accurate CFR synthesis. OptML exhibits heavier tails and MAE 0.18 rad and 2.23 rad, as UL-only conditioning struggles to capture geometry-induced phase relationships between UL and DL scatterers. Delay distributions (Fig. 6) exhibit the characteristic bimodality of urban ray-traced channels: a sharp peak near zero delay from LOS/direct paths and a longer multipath tail extending to 500 ns from reflections and diffractions. GNN-RAP faithfully reproduces this structure across both gaps, with predicted means within 69 ns (28 GHz) and 95 ns (300 GHz) of ground truth. OptML, lacking geometry awareness, systematically underestimates the multipath tail shifting mass toward shorter delays (means 253 ns and 218 ns), as it cannot infer scene-dependent long-range scattering from UL alone.

The distribution comparisons demonstrate that GNN-RAP learns realistic marginal path statistics across the full range of large-gap FDD scenarios, even at 300 GHz, where UL-DL congruence is minimal, as shown in Fig. 2. These marginal matches imply strong joint path fidelity: when paths have realistic angles, delays, phases, and powers individually, they are likely to form coherent multipath clusters and CFRs.

VI. Conclusion

Paper proposes predicting downlink (DL) paths in cross-band FDD with large frequency gaps up to 295 GHz. In this scenario, the uplink (UL) to DL correlation is very low, thus it

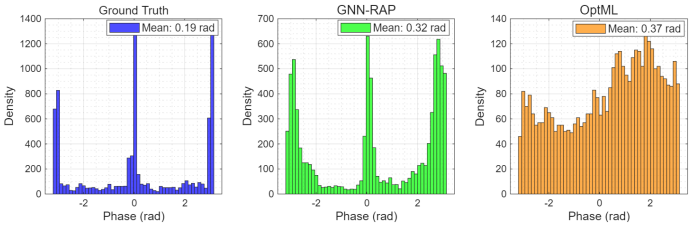

(a) Uplink: 3.5 GHz, Downlink: 28 GHz

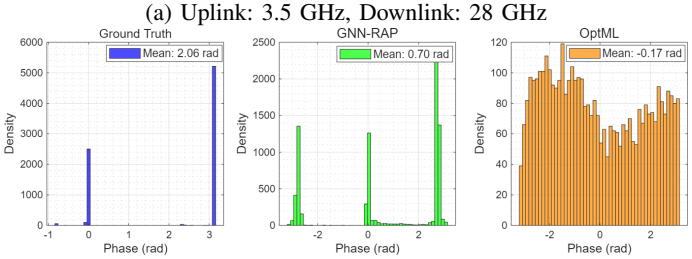

(b) Uplink: 3.5 GHz, Downlink: 300 GHz

Fig. 5: Path phase prediction distribution.

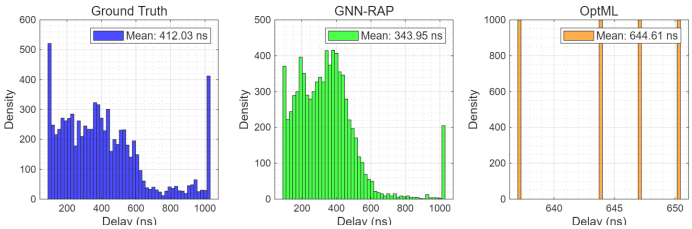

(a) Uplink: 3.5 GHz, Downlink: 28 GHz

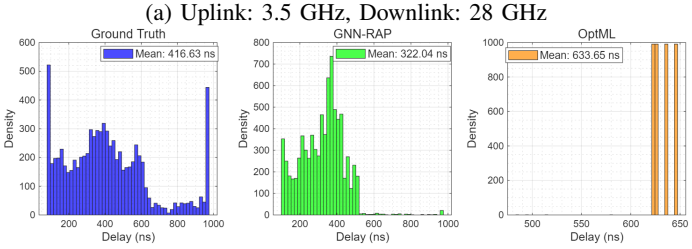

(b) Uplink: 3.5 GHz, Downlink: 300 GHz

Fig. 6: Path delay prediction distribution.

becomes complex to predict DL paths without any reference signals. Our proposed graph neural network for radio access paths demonstrates the viability and effectiveness of graph neural networks for predicting DL propagation paths from UL channel measurements and environment information. We were able to capture almost 90% of DL power as compared to true paths, as opposed to OptML having large errors. Similarly phase and delay distributions also show that GNN-RAP achieves the closest distributional match with lower MAE as compared to OptML. Thus, the GNN-RAP produces more accurate DL paths. Future work would explore scalability to larger antenna arrays. The methodologies developed and validated in this work provide a foundation for further exploration of learning-based channel prediction.

VII. Acknowledgements

This work was supported by the U.S. National Science Foundation (I-Corps, Award No. 2449098, 2025), Patuxent Riverkeeper (2025), the Kennesaw State University Office of Research (GRND8 Grand Challenges, 2025), and Shore Innovation Center, Kennesaw State University (2025).

References

[1] A. Bakshi, Y. Mao, K. Srinivasan, and S. Parthasarathy, "Fast and efficient cross band channel prediction using machine learning," in *The 25th Annual International Conference on Mobile Computing and Networking*, 2019, pp. 1–16.

[2] J. Hoydis, S. Cammerer, F. A. Aoudia, A. Vem, N. Binder, G. Marcus, and A. Keller, "Sionna: An open-source library for next-generation physical layer research," *arXiv preprint arXiv:2203.11854*, 2022.

[3] O. Kanhere and T. S. Rappaport, "Calibration of nyuray, a 3d mmwave and sub-thz ray tracer using indoor, outdoor, and factory channel measurements," in *ICC 2023-IEEE International Conference on Communications*. IEEE, 2023, pp. 5054–5059.

[4] M. Lecci, P. Testolina, M. Giordani, M. Polese, T. Ropitault, C. Gentile, N. Varshney, A. Bodi, and M. Zorzi, "Simplified ray tracing for the millimeter wave channel: A performance evaluation," in *2020 Information Theory and Applications Workshop (ITA)*. IEEE, 2020, pp. 1–6.

[5] A. Zubow, S. Rösler, and F. Dressler, "Ns3sionna: Realistic wireless network simulation with ray tracing in ns-3."

[6] S. Sharma, P. K. Singya, K. Deka, C. Adjih, and M. Sharma, "Terahertz communication: State-of-the-art and future directions," *IEEE Open Journal of the Communications Society*, 2025.

[7] Z. Zhang, J. Zhang, Y. Zhang, L. Yu, and G. Liu, "Ai-based time-, frequency-, and space-domain channel extrapolation for 6g: Opportunities and challenges," *IEEE Vehicular Technology Magazine*, vol. 18, no. 1, pp. 29–39, 2023.

[8] T. Orekondy, P. Kumar, S. Kadambi, H. Ye, J. Soriaga, and A. Behboodi, "Winert: Towards neural ray tracing for wireless channel modelling and differentiable simulations," in *The Eleventh International Conference on Learning Representations*, 2023.

[9] F. J. Somolinos-Simón, A. Murg, H. Liu, C. J. Hellín, J. Gómez, and A. Tayebi, "A neural approach to ray tracing for realistic wireless channel simulation in indoor and urban scenarios."

[10] C. J. Vaca-Rubio, L. Blanco, R. Pereira, and M. Caus, "Kolmogorov-arnold networks (kans) for time series analysis," in *2024 IEEE Globecom Workshops (GC Wkshps)*. IEEE, 2024, pp. 1–6.

[11] K. Bian, M. Tao, and S. Sun, "Generalizable neural ray tracing towards physics-informed intelligent channel modeling," in *2025 IEEE/CIC International Conference on Communications in China (ICCC)*. IEEE, 2025, pp. 1–6.

[12] D. Vasisht, S. Kumar, H. Rahul, and D. Katabi, "Eliminating channel feedback in next-generation cellular networks," in *Proceedings of the 2016 ACM SIGCOMM Conference*, 2016, pp. 398–411.

[13] A. Banerjee, X. Zhao, V. Chhabra, K. Srinivasan, and S. Parthasarathy, "Horcrux: Accurate cross band channel prediction," in *Proceedings of the 30th Annual International Conference on Mobile Computing and Networking*, 2024, pp. 1–15.

[14] T. S. Rappaport, *Wireless communications: Principles and practice, 2/E*. Pearson Education India, 2010.

[15] T. L. Marzetta, E. G. Larsson, H. Yang, and H. Q. Ngo, *Fundamentals of massive MIMO*. Cambridge University Press, 2016.

[16] Z. Yuan, Y. Lyu, J. Zhang, P. Tang, X. Liu, J. Lin, S. S. Petersen, and W. Fan, "Sub-thz ray tracing simulation and experimental validation for indoor scenarios," in *2023 IEEE International Mediterranean Conference on Communications and Networking (MeditCom)*. IEEE, 2023, pp. 7–11.

[17] S. Bakirtzis, P. Almasan, J. Suárez-Varela, G. O. Ferreira, M. Kalntis, A. F. Zanella, I. Wassell, and A. Lutu, "Radio propagation modelling: To differentiate or to deep learn, that is the question," *arXiv preprint arXiv:2509.19337*, 2025.

[18] M. Alrabeiah and A. Alkhateeb, "Deep learning for tdd and fdd massive mimo: Mapping channels in space and frequency," in *2019 53rd asilomar conference on signals, systems, and computers*. IEEE, 2019, pp. 1465–1470.

[19] M. Meliha, "Approches de prédiction de canal basées sur l'ia/ml pour les réseaux b5g," Ph.D. dissertation, Nantes Université, 2025.